



Controlled chamber formation of per- and polyfluoroalkyl substances (PFAS) aerosols with *Pseudomonas fluorescens*: size distributions, effects, and inhalation deposition potential

Ivan Kourtchev¹, Steve Coupe¹, Allison Buckley², Jishnu Pandamkulangara Kizhakkethil¹, Elena Gatta³, Dario Massabò^{3,4}, Paolo Prati^{3,4}, Virginia Vernocchi⁴, and Federico Mazzei^{3,4}

¹Centre for Agroecology Water and Resilience (CAWR), Coventry University, Wolston Lane, Ryton on Dunsmore, CV8 3LG, UK

²Toxicology Department, Radiation, Chemical, Climate and Environmental Hazards Directorate, UK Health Security Agency, Harwell Campus, Chilton, Oxfordshire, OX11 0RQ, UK

³Dipartimento di Fisica, Università di Genova, Genoa, Italy

⁴Istituto Nazionale di Fisica Nucleare (INFN), Sezione di Genova, Genoa, Italy

Correspondence to: Ivan Kourtchev (ivan.kourtchev@coventry.ac.uk)

Abstract. Per- and polyfluoroalkyl substances (PFAS) are recognised as atmospheric contaminants, yet processes governing their aerosol formation, size distribution, and interactions with atmospheric particle surfaces remain unknown. We investigated aerosolisation and size-resolved behaviour of 25 PFAS covering short-, medium-, and long-chain perfluoroalkyl carboxylic acids (PFCA), perfluoroalkane sulfonates, fluorotelomer sulfonates and emerging alternatives. Experiments were conducted under controlled chamber conditions using a water–organic solvent system, in the absence/presence of the model bacterium *Pseudomonas fluorescens* seed, representative of wastewater-impacted environments. Most PFAS exhibited unimodal mass–size distributions peaking at 0.3 μm , indicating dominant association with the fine mode. Sulfonated PFAS showed broadly similar aerosol-phase concentrations regardless of carbon-chain length, whereas PFCA displayed increasing aerosolisation with chain length. Perfluorooctane sulfonic acid (PFOS) showed additional ultrafine enrichment, 6:2 fluorotelomer sulfonate (6:2 FTS) and sodium 4,8-dioxa-3H-perfluorononanoate (NaDONA) exhibited broader size profiles, suggesting compound-specific effects linked to volatility and interfacial behaviour. *Pseudomonas fluorescens* seed did not enhance PFAS aerosol concentrations through condensation or heterogeneous uptake onto bacterial particles or shift in modal diameters, and no enrichment was observed at bacterial size mode, indicating limited PFAS–bioaerosol association under the tested conditions. Multiple-Path Particle Dosimetry (MPPD) modelling based on the measured size distributions predicted substantial deposition of the aerosol-bound PFAS in the pulmonary region, particularly for compounds enriched in ultrafine particles. Our findings indicate that PFAS aerosol behaviour in mixed-solvent systems is controlled primarily by physical droplet generation and evaporation, with implications for airborne transport and inhalation exposure from contaminated aqueous sources.



30 1 Introduction

31 Per- and polyfluoroalkyl substances (PFAS) are synthetic organofluorine compounds widely used in industrial and consumer
32 applications due to their high thermal stability and strong surface-active behaviour (Glüge et al., 2020). Their persistence,
33 mobility, and potential toxicity have raised growing environmental and health concerns, particularly given their ubiquitous
34 presence in water, soil, and the atmosphere (see reviews Evich et al., 2022; Faust, 2023). Atmospheric transport is now
35 recognised as an important pathway for the redistribution of PFAS on regional and global scales (Barber et al., 2007; Ellis et
36 al., 2004; Kourtchev et al., 2024; Kourtchev et al., 2025; Schenker et al., 2008), yet the mechanisms by which these compounds
37 enter and are stabilised in the atmospheric particle phase remain poorly understood.

38 PFAS are surfactants that readily accumulate at air–water interfaces (Schaefer et al., 2019) and adsorb onto mineral (Alves et
39 al., 2020; Folorunsho et al., 2025), organic (Wanzen et al., 2023), and biological surfaces (Dai et al., 2023). Their strong
40 interfacial activity suggests that pre-existing airborne particles could act as carriers or “seeds” for PFAS, facilitating their
41 transfer from aqueous systems into the atmosphere. Laboratory studies with sea-spray aerosol have shown that PFAS
42 enrichment in surface films exceeds that of bulk water by several orders of magnitude (Johansson et al., 2019), supporting the
43 likelihood of interfacial transfer. In the atmosphere, aerosol particles can grow through the condensation of semi-volatile
44 compounds when ambient vapour pressures fall below equilibrium values, leading to vapour uptake by existing particles
45 (Romakkaniemi et al., 2011; Stolzenburg et al., 2018). The rate and extent of condensation depend on compound volatility,
46 surface tension, and relative humidity, as well as particle composition. For surface-active species such as PFAS, adsorption or
47 condensation at particle interfaces may not only contribute to particle growth but also promote their association with pre-
48 existing aerosols, effectively turning these particles into carriers for atmospheric transport. Interactions with organic or
49 biological material may further modify these processes by altering surface energy, hygroscopicity, and the stability of particle-
50 bound PFAS. Wastewater treatment plants (WWTPs) are of particular interest in this context, as they are recognised co-sources
51 of both PFAS (Cookson & Detwiler, 2022) and biological aerosols, also known as bioaerosol (Li et al., 2016; Poopedi et al.,
52 2025; Xu et al., 2020). During aeration and mechanical agitation, fine droplets containing PFAS and microbial material can
53 become airborne, providing a direct mechanism for PFAS transfer from water to air. Elevated concentrations of PFAS are
54 frequently detected in WWTP effluents and sludges (Cookson & Detwiler, 2022), and both PFAS and bioaerosol emissions
55 from aeration tanks are well documented (Ahrens et al., 2011; Li et al., 2016; Lin et al., 2022; Pandamkulangara Kizhakkethil
56 et al., 2025; Poopedi et al., 2025; Shoeib et al., 2016; Xu et al., 2020).

57 Despite growing evidence for PFAS volatilisation and enrichment during water-to-air transfer (Ahrens et al., 2011; Lin et al.,
58 2022; Pandamkulangara Kizhakkethil & Kourtchev, 2025; Pandamkulangara Kizhakkethil et al., 2024; Shoeib et al., 2016),
59 the potential involvement of biological aerosol particles in facilitating PFAS aerosolisation remains unexplored. Literature
60 indicates that bioaerosols can participate in heterogeneous chemical processes (e.g., Ervens & Amato, 2020; Estillore et al.,
61 2016), suggesting that similar behaviour may occur for PFAS. Recent work has shown that PFAS can associate with bacterial
62 cells, primarily through adsorption to cell surfaces and, to a lesser extent, through limited uptake into cell interiors (Dai et al.,



2023). Controlled batch and miscible-displacement studies using *Pseudomonas aeruginosa* (Gram-negative) and *Bacillus subtilis* (Gram-positive) demonstrated substantial retention and increased retardation of perfluorooctane sulfonic acid (PFOS), one of the most studied PFAS, in bacterial-inoculated porous media. While these observations are derived from aqueous and porous-media systems and cannot be directly extrapolated to the atmosphere, they provide a useful conceptual analogue: if bacterial cell surfaces in water promote PFAS association, analogous surface-mediated interactions could, in principle, occur with airborne biological particles. To date, however, no studies have examined PFAS interactions with bioaerosols in the atmospheric context, highlighting a clear and unaddressed research gap. In principle, microbial cells or their fragments could either enhance PFAS partitioning into the particle phase through sorptive or condensation processes or inhibit it via electrostatic or interfacial competition.

Understanding whether and how biological matter influences PFAS aerosol behaviour is therefore essential for accurately assessing emission pathways from engineered systems such as WWTPs. Furthermore, PFAS–bioaerosol interactions may alter the hygroscopicity and atmospheric lifetime of emitted particles, with implications for transport and deposition. A further uncertainty concerns the atmospheric transport, deposition, and human exposure potential of PFAS, all of which are intrinsically linked to particle size. Particle size governs the residence time and dispersal range of aerosols (Finlayson-Pitts and Pitts, 2000), their efficiency of dry and wet deposition (Farmer et al., 2021) and likelihood of respiratory uptake (Tsuda et al., 2013). Smaller submicron particles ($<1\ \mu\text{m}$) have low gravitational settling velocities and long atmospheric residence times, allowing efficient transport over long distances, whereas coarse particles are more readily removed from the atmosphere near emission sources through sedimentation and impaction (Zhang and Vet, 2006). Particle size also governs deposition behaviour and associated health outcomes: fine and ultrafine particles can penetrate deep into the pulmonary region of respiratory systems and reach the alveoli, where they are linked to cardiovascular and respiratory morbidity (Pope III & Dockery, 2006), whereas coarse particles deposit mainly in the upper airways and have been shown to induce inflammation and allergic responses (Wu et al., 2018).

Despite its importance, size-resolved information on PFAS in aerosols remains scarce and not always in agreement (Dreyer et al., 2015; Ge et al., 2017; Guo et al., 2018; Harada et al., 2006; Lin et al., 2022). Some of these studies considered a limited number of PFAS, typically a few legacy compounds such as perfluorooctanoic acid (PFOA) and PFOS or employed samplers with only a few size fractions (e.g. $n=5$), which makes direct comparison with other studies difficult. For example, Dreyer et al. (2015) studied aerosol size distributions in a semi-rural area of Geestacht, Germany, using a Berner-type cascade impactor ($0.14\text{--}11.4\ \mu\text{m}$) and found PFOA mainly associated with ultrafine/submicron particles ($<0.14\ \mu\text{m}$; within the fine fraction), while PFOS showed enrichment in the supermicron range, particularly $1.4\text{--}3.8\ \mu\text{m}$. Ge et al. (2017) examined indoor and roadside aerosols in Tsukuba, Japan, using a five-stage nano-sampler, and reported ionic perfluoroalkyl carboxylic acids (PFCA) mainly associated with fine particles ($<0.5\ \mu\text{m}$) indoors, while PFOS was enriched in coarse roadside particles ($2.5\text{--}10\ \mu\text{m}$). Guo et al. (2018) investigated urban aerosols in Shanghai, China, during a haze period using an eight-stage air sampler, and observed bimodal distributions, with PFOA peaking in both fine ($0.4\text{--}2.1\ \mu\text{m}$) and coarse ($3.3\text{--}10\ \mu\text{m}$) modes, and PFOS largely associated with coarse particles. Lin et al. (2022) analysed aerosols near wastewater treatment plants and a landfill in



Hong Kong, China, using an eleven-stage MOUDI impactor (0.056–10 μm), and found site-dependent patterns: perfluorobutanoic acid (PFBA) and PFOA showed variable fine- and coarse-mode enrichment, perfluorobutanesulfonic acid (PFBS) was generally coarse-dominated, and PFOS consistently peaked in the 1–10 μm range. These studies provide important data on PFAS size distribution in aerosols; however, the available information remains too limited to establish general patterns or identify the controlling mechanisms. Controlled laboratory investigations, though constrained by simplified conditions and the absence of real-world variability, are therefore needed to disentangle the effects of PFAS molecular structure and interfacial behaviour from the physical processes governing aerosol formation and droplet drying. Such information is critical for improving atmospheric fate models and exposure assessments. The aim of this study was to advance understanding of PFAS aerosol formation and size distribution under controlled laboratory conditions, with particular focus on the potential role of bioaerosols as carriers. In this study, we explore how PFAS with varying carbon chain lengths and functional groups undergo aerosolisation, both in the absence and presence of the model bacterium *Pseudomonas fluorescens*. This bacterium was chosen as it is commonly detected in wastewater and wastewater-impacted matrices, having been isolated from WWTP influent and effluent (including species-level recovery of *Pseudomonas fluorescens*) and from raw sewage of municipal treatment plants (phage isolation targeting *Pseudomonas fluorescens*) (Luczkiewicz et al., 2015; Sillankorva et al., 2008). Moreover, it presents a low biosafety risk, being classified as a non-pathogenic, Risk Group 1 organism suitable for use in controlled laboratory experiments. Size-resolved PFAS aerosol concentrations were determined for both systems to assess the influence of molecular structure and biological material on particle-phase behaviour. To the best of our knowledge, this is the first study to directly investigate PFAS–bioaerosol interactions and resolve their mass size distribution from polar solvent systems under controlled laboratory conditions. The resulting mass–size distributions were then applied to the Multiple-Path Particle Dosimetry (MPPD) model to evaluate how aerosol size affects potential respiratory deposition and human exposure. Such modelling provides a quantitative context for interpreting the potential health relevance of observed PFAS size distributions.

2 Materials and methods

2.1 Experimental facility, setup, and conditions

The experiments were performed in the Chamber for Aerosol Modelling and Bio-aerosol Research (ChAMBRé) facility at the University of Genoa, Italy. The chamber is a stainless-steel vessel with an internal volume of 2.2 m^3 , designed for studies of particle generation, ageing, and interaction under controlled environmental conditions (Massabò et al., 2018). All the experiments were conducted at ambient pressure and in dark conditions. Temperature and humidity inside ChAMBRé were continuously monitored and maintained at 23 ± 3 °C and 40 ± 6 %, respectively. Before each experiment, ChAMBRé was evacuated using a composite pumping system (rotary and root pumps) to achieve an internal pressure of approximately 5×10^{-2} mbar. The reestablishment of atmospheric pressure was facilitated by introducing ambient air into the chamber using a five-stage filtration, purification, and drying intake system, which comprised an absolute



HEPA filter and a zeolite trap (Vernocchi et al., 2023). A Waveband Integrated Bioaerosol Sensor (WIBS-NEO, Droplet Measurement Technologies®) has been incorporated into the ChAMBRé particle monitoring system to quantify bio-aerosol concentration. The extensive data produced by the WIBS during the ChAMBRé experiments were analysed using custom software developed in Igor 8.0 (Wavemetrics, Inc.), designed to extract airborne bacteria/bioaerosol concentration and size distribution within the chamber as a function of time and fluorescence intensity. In parallel, total particle number and size distributions were monitored in real time using a Scanning Mobility Particle Sizer (SMPS 3938, TSI Inc.) equipped with a differential mobility analyser (DMA 3081A) and a condensation particle counter (CPC 3750) in the range from 18 to 500 nm and an Optical Particle Sizer (OPS, TSI 3330) covering 0.3–10 µm range.

2.2 Aerosol generation and introduction

2.2.1 PFAS-only experiments

A mixed standard solution containing 25 PFAS was prepared using the EPA-533PAR native analyte mixture supplied by Wellington Laboratories (Ontario, Canada). The mixture comprised a broad suite of ionic PFAS, including perfluoroalkyl carboxylic acids (PFCA; C₄–C₁₂), perfluoroalkane sulfonates (PFSA; C₄, C₅, C₇ linear, and both linear and branched isomers of C₆ and C₈), and several fluorotelomer sulfonates and emerging replacement compounds. Specifically, the analyte mixture consisted of: 4:2 fluorotelomer sulfonate (4:2 FTS); 6:2 fluorotelomer sulfonate (6:2 FTS); 8:2 fluorotelomer sulfonate (8:2 FTS); hexafluoropropylene oxide dimer acid (HFPO-DA); perfluoro(2-((6-chlorohexyl)oxy)ethanesulfonic acid) (9Cl-PF3ONS); perfluoro(2-ethoxyethane)sulfonic acid (PFEEESA); perfluoro-3-methoxypropanoic acid (PFMPA); perfluoro-3,6-dioxaheptanoic acid (3,6-OPFHpA); perfluoro-4-methoxybutanoic acid (PFMBA); perfluorobutane sulfonic acid (L-PFBS); perfluorobutanoic acid (PFBA); perfluorodecanoic acid (PFDA); perfluorododecanoic acid (PFDoA); perfluoroheptane sulfonic acid (L-PFHpS); perfluoroheptanoic acid (PFHpA); perfluorohexane sulfonic acid (PFHxS); perfluorohexanoic acid (PFHxA); perfluorooctane sulfonic acid (PFOS); perfluorooctanoic acid (PFOA); perfluorononanoic acid (PFNA); perfluoropentane sulfonic acid (L-PFPeS); perfluoropentanoic acid (PFPeA); perfluoroundecanoic acid (PFUdA); sodium dodecafluoro-3H-4,8-dioxanonoate (NaDONA); 11-chloroeicosafluoro-3-oxaundecane-1-sulfonic acid (11Cl-PF3OUdS). All compounds were diluted to a final concentration of 0.5 ng mL⁻¹ in a mixture of 40:60 (v/v) methanol and ultrapure water (18.2 MΩ cm) to ensure adequate solubility and minimise losses to container surfaces.

The addition of methanol (≥99.9% (GC), LiChrosolv®, Supelco) was necessary to prevent analyte loss due to sorption onto the nebuliser container walls and to improve the solubility of long-chain PFAS in water. Aerosols were generated using a three-jet Collison nebuliser operated at 5 L/min and introduced into ChAMBRé through a stainless-steel inlet connected directly to the chamber. Aerosol generation continued for 30 min, followed by a mixing period of 10 min before sampling, facilitated by the mixing fan installed at the base of the ChAMBRé. The internal fan was operated at 5 Hz, a setting shown by Massabò et al. (2018) to achieve complete mixing in the ChAMBRé within approximately 2 min. Experiments were repeated three times and are referred to as Exp 1-3 (no bacteria) below. Aerosol drying prior to chamber introduction was intentionally



avoided to minimise PFAS losses. PFAS are known to interact with surfaces and can partition during drying, so passing the aerosol through additional tubing or drying devices (e.g., diffusion dryers/denuders) would introduce unnecessary interfaces and increase the risk of losses. Introducing the wet aerosol directly into the chamber therefore ensured that the measured composition reflected primary aerosol generation rather than processing artefacts.

2.2.2 PFAS and *Pseudomonas fluorescens* experiments

The *Pseudomonas fluorescens* ATCC 13525 (obtained from the American Type Culture Collection, University Boulevard, Manassas, Virginia, United States) was grown in 30 mL volume of nutrient broth medium. The culture was incubated at 25°C with continuous shaking in a shaker incubator (SKI 4 ARGOLAB, Carpi, Modena, Italy) at 200 rpm. The growth curve was monitored by measuring the absorbance at $\lambda = 600$ nm using a spectrophotometer (Shimadzu 1900) until it reached the stationary phase (approximately 1) corresponding to about 109 cells mL⁻¹. Subsequently, 20 mL of the bacterial suspension was centrifuged at 5000 rpm for 10 min, and the cell pellet was resuspended in 20 mL of sterile Milli Q (MQ) water.

The bacteria in MQ were nebulised using Sparging Liquid Aerosol Generator (SLAG) (CH Technologies, USA) with a 0.75" diameter porous disc and nominal pore size of 2 μ m. 3 mL of the bacterial suspension with a syringe pump flowrate of 0.4 mL min⁻¹ were dripped onto the SLAG porous stainless-steel disk and nebulised inside ChAMBRe with a flowrate of 3.5 lpm as performed in previous experiments (Gatta et al., 2025).

Bioaerosol was allowed to mix for 5 min, followed by addition of PFAS in the same way as described in 2.2.1. Aerosol generation continued for 30 min, followed by a mixing period of 10 min before sampling. Experiments were repeated three times and are referred to as Exp 4-6 (with bacteria) below.

2.2.3 Blank experiments

Blank experiments were conducted to assess potential contamination or background levels arising from the experimental setup and to correct for any systematic bias in the measurements. A 40:60 (v/v) methanol–ultrapure water mixture without PFAS was nebulised using a Collison nebuliser at 5 L min⁻¹. Aerosol generation was maintained for 30 min, followed by a 10 min mixing period prior to sampling. All other experimental conditions were identical to those described in Section 2.2.1. The blank experiments were repeated three times.

2.3 Aerosol generation and introduction

Size-segregated aerosol samples were collected using a Nano Micro-Orifice Uniform Deposit Impactor (NanoMOUDI-IITM, Model 125B, MSP Corporation, USA) operated at a flow rate of 30 L min⁻¹. The NanoMOUDI provided aerodynamic cut-off diameters of 10.000, 5.600, 3.200, 1.800, 1.000, 0.560, 0.320, 0.180, 0.100, 0.056, 0.032, 0.018, and 0.010 μ m.

Total suspended particles (TSP) were collected in parallel with a double cone sampler, directly connected to ChAMBRe, at a flow rate 10 L min⁻¹. The total sampling duration for both NanoMOUDI and TSP was 2 hours.



191 PallFlex 2500 QAO-UP quartz fibre filters were used as substrates in both samplers. Due to the unavailability of PallFlex 2500
 192 QAO-UP filters for all experiments, quartz microfibre filters (RVMSFQ47Q90, Mega Systems s.r.l.) were used in TSP
 193 sampling in one of the replicate experiments involving bacteria. All filters were prebaked at 450 °C for 2.5 hours prior to
 194 sampling. Based on recoveries and variability between TSP replicates (RSD < 10%), which was not higher than that observed
 195 for replicates using the same filter type, the use of a different filter brand is expected to have a negligible impact on the results.
 196 Following sampling, aerosol samples were wrapped into aluminium foil (prebaked at 450 °C for 2 hours) avoiding contact
 197 with any plasticware and external environment and stored at –20 °C until extraction.

198 **2.4 PFAS extraction and analysis**

199 Samples generated in the chamber were extracted and analysed following the procedure described by Kourtchev et al. (2022).
 200 Briefly, filter edges in contact with the sampler gaskets were removed prior to extraction. Each filter was placed in a precleaned
 201 10 mL glass vial (Chromacol 10-HSV, Thermo Scientific) and spiked with 25 µL of an internal standard (IS) mixture
 202 containing 16 isotopically labelled (¹³C) PFAS at 1 ng mL⁻¹ and three telomer sulfonates (M2-4:2 FTS, M2-6:2 FTS, and M2-
 203 8:2 FTS) at 4 ng mL⁻¹. Full names of the isotopically labelled PFAS are shown in Table S1 of supplement. Samples were
 204 extracted twice with 5 mL of Liquid Chromatography Mass Spectrometry (LC-MS, CHROMASOLV™ ≥99.9%) grade
 205 methanol using ultrasonic agitation in a chilled water bath for a total of 40 min (2 × 20 min). The combined extracts were
 206 filtered through PTFE membrane filters (0.45 µm, Iso-Disc PTFE-13-4) into prewashed 10 mL glass vials (Chromacol 10-
 207 HSV) tightly closed with metal screw caps and PTFE septa (Chromacol 18-MSC and 18-ST101).

208 Extracts were then reduced in volume to 1 mL under a gentle stream of nitrogen and stored at 4 °C until analysis. On the day
 209 of analysis, 4 mL of Optima™ LC-MS grade water was added to each sample, which was subsequently vortex-mixed and
 210 analysed using online SPE consisting of an EQUAN MAX Plus Thermo Scientific™ Vanquish™ UHPLC system equipped with
 211 a Thermo Scientific™ TriPlus™ RSH autosampler, following the method described by Kourtchev et al. (2022).

212 Only PFAS detected above the method's LOD (Kourtchev et al., 2022) or above blank levels were considered in the data
 213 interpretation. All data were corrected for chamber dilution to account for the continuous inflow of clean air required to
 214 maintain stable chamber pressure. No correction was applied for potential chamber wall losses. Because the chamber and
 215 associated lines are made of stainless steel, and long-chain PFAS are known to interact strongly with metal surfaces, additional
 216 losses to the walls are likely and may contribute to the overall uncertainty. However, as all experiments were conducted under
 217 the same conditions, any wall-loss effects are expected to be systematic and should not affect the relative comparison of the
 218 results.

219 **2.5 Multiple-Path Particle Dosimetry (MPPD) modelling**

220 For each region of the human respiratory tract (Head, Tracheobronchial region (TB) and Pulmonary region(P), the deposition
 221 efficiency as a function of particle size, was estimated using the MPPD model (version 2.11, Applied Research Associates,
 222 Inc.) (Anjilvel & Asgharian, 1995), using the default human breathing parameters (further details and results are provided in



the supplement file). The MPPD model is based on a framework of semiempirical equations and computational algorithms that simulates particle deposition in the respiratory tract using anatomical and physiological data. It accounts for species-specific airway geometry, breathing patterns, and particle characteristics to estimate regional and total deposition under various exposure scenarios.

The deposition flux, $DF_{r,i}$ (pg h^{-1}) to each region of the human respiratory tract (Head, TB or Pulmonary), r , for each nanoMOUDI size bin, i (assuming constant exposure), was then calculated as

$$DF_{r,i} = DE_{r,i} \times C_i \times V$$

where $DE_{r,i}$ is the deposition efficiency, C_i (pg m^{-3}) is the measured concentration of the target PFAS and V ($\text{m}^3 \text{h}^{-1}$) is the human breathing rate. The deposition fluxes for the coarse ($> 2.5 \mu\text{m}$), fine ($0.1 - 2.5 \mu\text{m}$), and ultrafine ($< 0.1 \mu\text{m}$) size fractions were then calculated by summing across the relevant MOUDI size bins.

3 Results and Discussions

3.1 Total suspended particles (TSP)

Figure 1 shows concentration of individual PFAS measured in the TSP fraction for the PFAS-only (Exp 1–3) and PFAS with *Pseudomonas fluorescens* seeded (Exp 4–6) experiments.

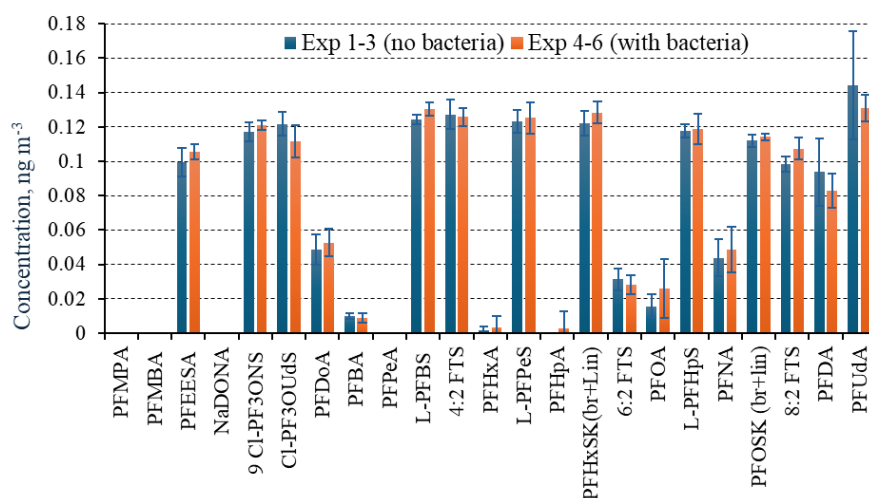
Distinct trends were observed between the sulfonated and carboxylated PFAS. The sulfonated compounds, i.e. PFBS, PFHxS, PFOS, and the fluorotelomer sulfonates (4:2, 6:2, and 8:2 FTS), exhibited relatively uniform aerosol-phase concentrations, indicating that chain length had little influence on their aerosolisation efficiency. Their consistent behaviour likely reflects the inherently high surface activity of sulfonates, which promotes their enrichment at the air water interface (Klevan et al., 2025; Lyu et al., 2022).

In contrast, the PFCA showed a clear chain-length dependence, with aerosol-phase concentrations increasing from PFBA to PFUDA. In a 40:60 methanol-water system, methanol decreases surface tension and solvent polarity, enhancing the solubility and mobility of longer-chain PFCA relative to pure water (Kutsuna et al., 2012). This mixed-solvent environment therefore favours the transfer of hydrophobic carboxylates into the aerosol phase. It must be noted that short-chain PFAS e.g. PFBA (C_3) are less surface active and can remain in solution (Cai et al., 2022; Klevan et al., 2025).

Accordingly, sulfonated PFAS appear dominated by interfacial adsorption, whereas carboxylated PFAS are more strongly affected by bulk-phase solvation governed by solvent composition. While direct comparison with earlier studies is limited by methodological differences, similar behaviour has been observed during water aeration, where perfluoro sulfonated compounds exhibited higher aerosolisation efficiencies than carboxylated analogues (Pandamkulangara Kizhakkethil et al., 2024; Pandamkulangara Kizhakkethil and Kourtchev, 2025). A similar trend, involving an increase in aerosol-phase perfluorinated alkyl acids, their salts and conjugate bases abundance with perfluoroalkyl chain length but not equivalent

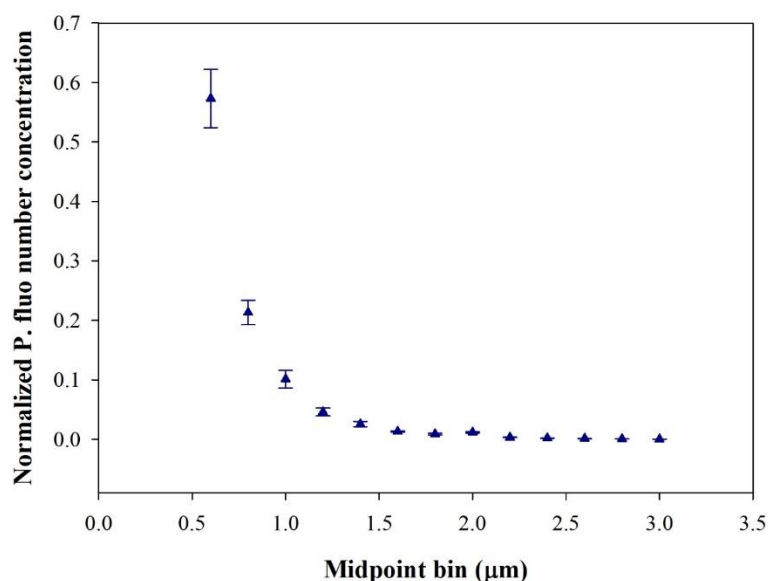


253 enrichment magnitudes, was also observed under highly aqueous (tap water) conditions in bubble-bursting experiments using
 254 a plunging jet, which is considered representative of nascent sea spray aerosol formation, as reported by Reth et al. (2011).
 255 In the presence of *Pseudomonas fluorescens* (Fig. 1, Exp 4–6), the overall TSP concentrations of most PFAS were comparable
 256 to those in the PFAS-only experiments, indicating that bacterial seeds did not substantially influence PFAS aerosolisation
 257 under the tested conditions. The average and standard deviation of bacteria concentration across the 3 replicated experiments,
 258 measured by WIBS, 5 minutes after the end of injection was $29 \pm 1 \text{ \# cm}^{-3}$. Slight reductions observed for some long-chain
 259 PFCA (e.g. PFNA, PFDA, PFUdA) may reflect weak sorptive interactions with bacterial cell walls or their fragments, although
 260 these effects appear minor relative to the dominant physicochemical controls. The overlap of standard deviations between the
 261 two experimental conditions (with and without *Pseudomonas fluorescens*) suggests that PFAS concentrations in aerosol were
 262 similar within the experimental uncertainty.
 263 It must be noted that the major fraction of *Pseudomonas fluorescens* present in the chamber was observed around 0.6 \mu m
 264 (Figure 2), smaller than the typical bacterial dimension (about $2\text{--}4 \text{ \mu m}$ in length and $0.5\text{--}1.0 \text{ \mu m}$ in diameter). It is worth noting
 265 that the nebulisation processes exert stress on bacteria, producing fragmentation (Park et al., 2009). Particles in this size range
 266 lie within the accumulation mode and therefore may act as efficient condensation sinks for condensable species (Engvall et
 267 al., 2008). In the present experiments, PFAS were introduced in ionic form via nebulisation, yielding PFAS in both the gas
 268 phase and the particle phase (the latter associated with nebulised droplets and their dried residues). Any enrichment of PFAS
 269 on the pre-existing bacterial particles would therefore have required gas–particle partitioning to the bacterial surface or
 270 particle–particle interactions such as coagulation. The absence of measurable enhancement in PFAS aerosol concentrations
 271 therefore suggests that condensation or adsorption of PFAS onto bacterial surfaces was not thermodynamically favourable, or
 272 that kinetic limitations prevented significant mass transfer during the experimental timescale. This suggests that, under the
 273 applied conditions, PFAS aerosol formation and growth were predominantly governed by nebulisation and subsequent droplet
 274 drying processes rather than by heterogeneous uptake onto biological particles.





276 **Figure 1: Aerosol-phase concentrations of individual PFAS measured in total suspended particles (TSP) during PFAS-only**
 277 **experiments (Exp 1–3, blue) and PFAS + *Pseudomonas fluorescens*-seeded experiments (Exp 4–6, orange). Error bars show the**
 278 **standard deviation across three chamber replicates with duplicate LC–MS analyses per replicate (n = 6).**



279
 280 **Figure 2: Normalised particle size distribution of *Pseudomonas fluorescens* nebulised in ChAMBRé (5 minutes after the end of**
 281 **bacteria nebulisation). Data represent the mean ± standard deviation of three replicate experiments.**

282 3.2 Mass–Size Distributions of PFAS

283 As mentioned in the Methodology section, not all PFAS detected in the TSP samples were also observed in the NanoMOUDI
 284 samples, with carboxylated PFAS being mainly affected. This was likely due to their lower aerosol concentrations in the
 285 chamber (as also observed in TSP) and their generally higher volatility (e.g. PFBA, 6.37 mmHg at 25 °C, Steele et al., 2002;
 286 PFHxA, 13 mmHg at 25 °C, US EPA, 2012), which reduce particle-phase partitioning. Additionally, “dilution” across multiple
 287 MOUDI stages may have further contributed to concentrations falling below the LC-MS detection limit in the NanoMOUDI
 288 samples.

289 The majority of PFAS (excluding 6:2 FTS and PFOS) aerosols exhibited a consistent unimodal mass–size distribution, peaking
 290 at 0.32 μm (Figure 3). Interestingly, variations in the molecular composition of the tested PFAS, including differences in
 291 perfluorocarbon chain length and terminal functional group, did not affect the mode diameter of the aerosol mass–size
 292 distribution. PFAS, representing a broad range of compounds, differ markedly in hydrophobicity and interfacial activity as a
 293 function of both chain length and functional group (e.g. Lyu et al., 2022; Patel et al., 2024; Leung et al., 2023), which makes
 294 the present observation somewhat unexpected. For instance, long-chain sulfonates such as PFOS (C8) exhibit considerably
 295 stronger surface activity than short-chain carboxylates such as PFBA (C3), and their behaviour in bulk aqueous systems differs
 296 accordingly (Guo et al., 2023).



297 This suggests that, under the applied experimental conditions, aerosol formation and size characteristics were largely governed
298 by physical processes. The most plausible explanation is that the aerosol-generation method imposed uniform physical
299 constraints during droplet formation and solvent evaporation, limiting the extent to which molecular properties influenced
300 particle characteristics. In addition, the use of an organic solvent likely enhanced the solubility of all PFAS, including long-
301 chain species with low water solubility, allowing them to remain in solution and aerosolise more uniformly during nebulisation.
302 Methanol substantially reduces surface tension (from 71.7 dyne cm⁻¹ for pure water to 38.7 dyne cm⁻¹ at 40 % v/v methanol
303 at 25 °C; Cheong and Carr, 1987), which promotes droplet formation and minimises differences in surface activity among
304 PFAS, thereby obscuring potential molecular-specific effects on aerosol behaviour.

305 The two analytes, 6:2 FTS and PFOS, did not follow the general mass-size distribution trend. Although PFOS exhibited a
306 dominant submicron mass mode at 0.32 µm, similar to other PFAS, its mass-size profile showed a relatively larger fraction of
307 mass in the smallest measured bins. In other words, PFOS retained the common 0.32-µm residual peak but also displayed
308 enrichment in the ultrafine fraction compared with other PFAS in the mixture. PFOS may produce a larger fraction of ultrafine
309 aerosol particles than other PFAS due to its greater surface activity (Klevan et al., 2025; Lyu et al., 2022). Although the
310 presence of methanol substantially reduces bulk surface tension, PFOS can still dominate dynamic interfacial processes during
311 rapid droplet formation. Its strong and persistent adsorption at the air–liquid interface, combined with enrichment as methanol
312 evaporates, likely lowers local surface tension further and inhibits coalescence, resulting in smaller and more stable droplets.
313 In addition, the anionic nature of PFOS may contribute to electrostatic stabilisation of charged droplets, further enhancing the
314 ultrafine fraction.

315 Other long-chain PFAS in the mixture did not exhibit similar enrichment, potentially due to competitive adsorption and
316 intermolecular interactions in mixtures that modulate their effective surface activity.

317 Only a limited number of studies have reported size-resolved mass distributions of PFAS associated with atmospheric particles
318 from the field observations. Comparison with previous work shows that PFAS size distributions vary considerably among
319 studies. Harada et al. (2006) and Dreyer et al. (2015) reported compound-dependent patterns, with PFOA and other PFCA
320 enriched in fine or ultrafine particles, whereas PFOS tended to occur in coarser fractions. In contrast, Guo et al. (2018) found
321 both PFOA and PFOS primarily associated with fine particles (< 1 µm), while Ge et al. (2017) observed PFCA in ultrafine
322 particles (< 0.1 µm) and PFOS and other sulfonates in coarse modes. Such variability likely reflects differences in sources,
323 atmospheric conditions, and sampling methodologies, as well as local physicochemical environments influencing PFAS
324 partitioning.

325 To the best of our knowledge, previous laboratory investigations of PFAS aerosol size behaviour have focused primarily on
326 sea-spray systems, which are not directly comparable to the organic solvent-rich aerosolisation process examined here.
327 Johansson et al. (2019) reported that the highest enrichment of perfluoroalkyl acids (PFAA) relative to seawater occurred in
328 aerosols with aerodynamic diameters below 1.6 µm. Sha et al. (2021) found that particle surface-area-to-volume ratio was a
329 strong predictor of PFAS enrichment in supermicron particles but not in submicron particles, indicating that different physical
330 controls operate across size ranges. In their subsequent work, Sha et al. (2024) observed that PFAS enrichment was particularly



pronounced in submicrometer sea-spray aerosol particles and varied with chain length and dissolved organic matter content. These studies suggest that in marine systems, PFAS enrichment and size association are sensitive to experimental conditions and molecular structure, with both particle-scale physics and surfactant properties influencing partitioning. In contrast, the consistent submicron unimodal distribution observed in the present work likely reflects aerosol formation under organic-solvent conditions, where rapid solvent evaporation and solute concentration effects impose dominant physical constraints that reduce the influence of PFAS molecular features on particle size.

The introduction of *Pseudomonas fluorescens* into the chamber as a potential seed or carrier of PFAS, in most cases, had either no effect (within experimental error) or resulted in a uniform decrease in PFAS aerosol mass size concentration across nearly the entire size range for two analytes (i.e. PFEESA and GenX), while the distribution profile and modal diameter remained unchanged. As mentioned in the section 3.1, the major fraction of *Pseudomonas fluorescens* in the chamber was observed around 0.6 μm (Fig 2). The absence of PFAS enrichment at the bacterial modal size ($\sim 0.6 \mu\text{m}$) and the unchanged PFAS modal diameter ($\sim 0.3 \mu\text{m}$) indicate that *Pseudomonas fluorescens* did not noticeably influence PFAS size distribution under the tested conditions. This was somewhat unexpected, as PFAS have been shown to associate with bacterial surfaces in aqueous systems (Dai et al., 2023). The physicochemical environment in aerosols likely may differ from that in bulk water. The outer membrane of *Pseudomonas fluorescens* carries a net negative charge, arising from acidic functional groups on lipopolysaccharides and phospholipids (Boyd Chelsea et al., 2014; Charlton et al., 2024), while the tested PFAS are also anionic. Such electrostatic repulsion could therefore further inhibit PFAS attachment, potentially explaining the absence of observable enrichment at $\sim 0.6 \mu\text{m}$. In addition, although PFAS are amphiphilic, their molecular structure makes the air–water interface far more favourable for stabilisation than the hydrated, negatively charged bacterial surface, and PFAS therefore likely preferentially stabilise at droplet interfaces rather than adsorb onto bacterial cells. Another aspect worth considering is whether *Pseudomonas fluorescens* could have influenced PFAS aerosol concentrations through biochemical transformation rather than solely through physical carrier processes. In bulk aqueous systems, several *Pseudomonas* species have been reported to partially degrade sulfonated PFAS, particularly precursors such as H-PFOS, under nutrient-enriched or co-metabolic conditions (e.g., Key et al., 1998). The latter work involved liquid culture media with high bacterial densities, organic carbon co-substrates, and prolonged incubation times, which facilitate enzymatic activity and redox transformations. However, even in that study, evidence for complete degradation of PFOS is lacking; rather, transformation is slow, partial, and often requires co-metabolic drivers. By contrast, the conditions in our aerosol chamber differ fundamentally. The bacteria were suspended in air with transient water content ($\text{RH} \sim 40\%$), rather than immersed in nutrient-rich aqueous media. Under such conditions, the metabolic activity of *Pseudomonas fluorescens* is expected to be extremely limited. The observed uniform decrease in PFAS aerosol mass concentration cannot therefore be straightforwardly attributed to microbial degradation, as the air–water interface-dominated microenvironment is unlikely to sustain enzymatic pathways known to act on PFAS in bulk liquid cultures. Furthermore, the residence time of particles in the chamber is orders of magnitude shorter than the timescales over which reported PFAS transformations by *Pseudomonas* occur (days to weeks). It is therefore more plausible that the apparent decrease in GenX and PFEESA aerosol mass concentrations reflect non-biological processes such as redistribution of material to



365 chamber or sampler walls, or surface-competition dynamics during condensation, rather than direct microbial influence. If any
366 biochemical contribution occurred, it would likely be negligible compared with these physicochemical pathways. The
367 difference in TSP concentrations between the *Pseudomonas fluorescens*-seeded (average 0.105 ± 0.0043 ng m⁻³, n=3) and
368 unseeded (0.099 ± 0.008 ng m⁻³, n=3) experiments for PFEESA was minimal, suggesting that the concentration drop observed
369 in the NanoMOUDI size-resolved data likely resulted from sampling artefacts or volatility-driven size redistribution rather
370 than bacterial activity. In this respect, it has been shown that compounds with higher volatility tend to exhibit greater mass
371 losses through evaporation particularly in impactor-based sampling systems like NanoMOUDI (e.g. Ungeheuer et al., 2022).
372 Although the same inferences could not be made for GenX from the TSP data, due to high background levels in the TSP
373 blanks, evaporation from the collection substrate in the NanoMOUDI was likely the dominant loss process, as also suggested
374 for PFEESA. The relatively high vapour pressure of GenX (2.7 mm Hg at 20 °C, US EPA, 2022) supports this interpretation.
375 In previous work, it was found that the culturable lifetime of *P. fluorescens* in ChAMBRé in dark condition was about 20
376 minutes (Gatta et al. 2025). Furthermore, the survival of bacteria in air is known to be sensitive to aerosolisation and sampling
377 conditions rather than simply liquid-phase growth (Després et al., 2012; Hong et al., 2021). It must be noted that in our study
378 the bacteria were seeded in sterilised MQ, whereas PFAS were introduced separately via a 40:60 (v/v) methanol-water
379 nebulisation. Under this experimental setup, bacteria were not subjected to high alcohol strength in the droplet phase; instead,
380 their methanol exposure was dominated by chamber-average vapour and sporadic interactions near the spray plume. These
381 conditions are unlikely to produce strong biocidal effects at the population level, so the absence of PFAS enrichment at the
382 bacterial size mode is better explained by interfacial/partitioning constraints than by methanol-induced loss of viability.
383 Moreover, even if a fraction of the bacterial population experienced viability loss, this would not preclude potential PFAS
384 interactions with biological surfaces. Non-viable bacterial cells, cell-wall fragments, and microbial biomass retain abundant
385 functional groups (carboxyl, phosphate, and amine moieties) known to sorb organic and inorganic species (Fathollahi & Coupe,
386 2021; Torres, 2020; Wang & Chen, 2009). Inactivated bacterial biomass is widely used as a biosorbent due to preserved surface
387 chemistry and polymeric matrices (Torres 2020). In the atmosphere, biological particles occur not only as intact cells but also
388 as cell fragments and exudates (Després et al., 2012; Fröhlich-Nowoisky et al., 2016), meaning that surface area and chemical
389 functionality persist even when viability is compromised. Thus, even partial loss of viability would still permit association of
390 PFAS with microbial surfaces if interfacial partitioning were favourable. The lack of detectable PFAS at the bacterial size
391 mode therefore reinforces that limited affinity/partitioning, rather than loss of cellular integrity, governed PFAS–bioaerosol
392 interactions under our experimental conditions.
393

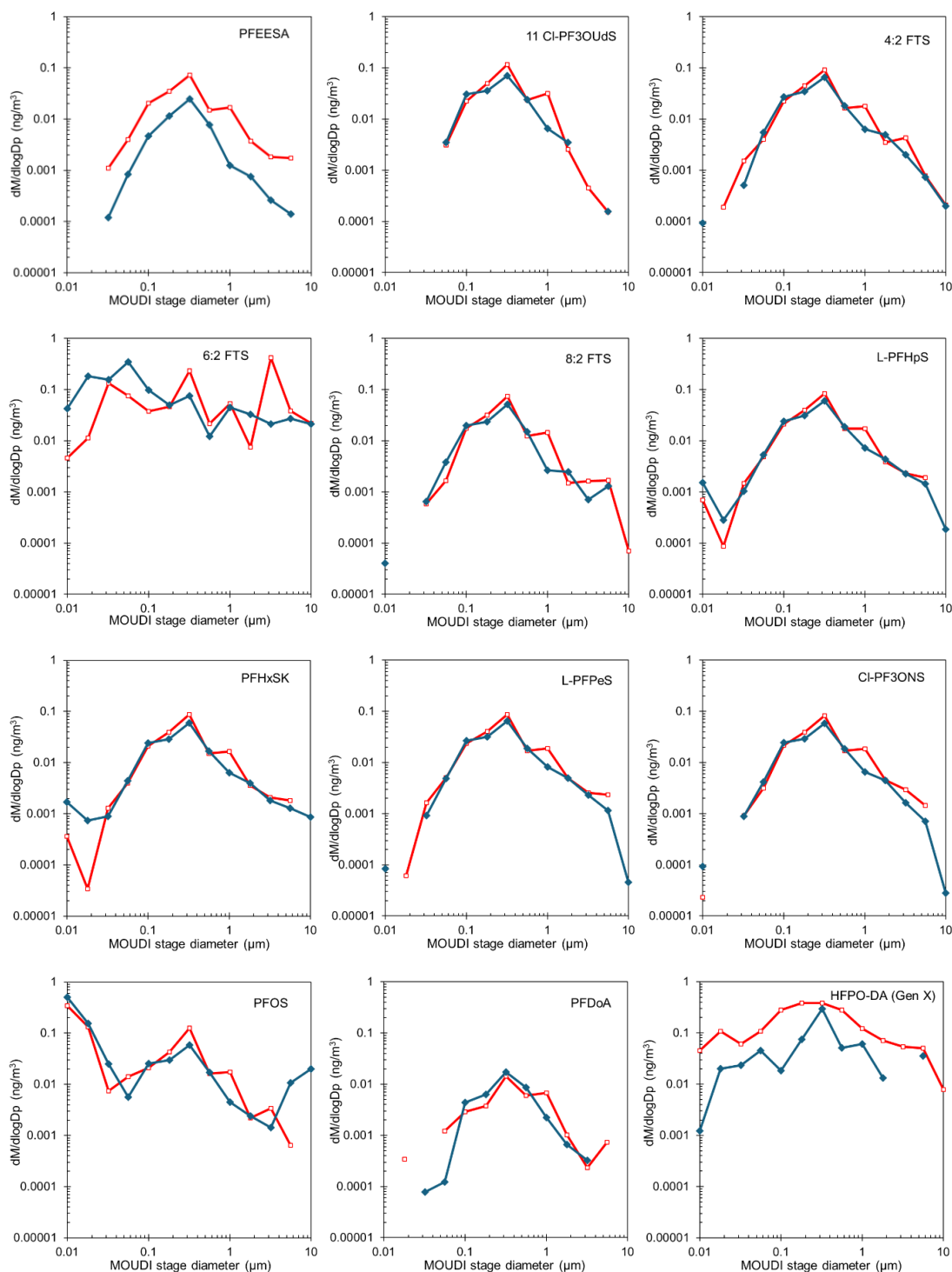




Figure 3: Mass size distribution of aerosol from PFAS-only (blue symbols) and PFAS with *Pseudomonas fluorescens* seed (red symbols) experiments.

3.3 Multiple-Path Particle Dosimetry (MPPD) modelling

Figure 4 (with data given in the supplement) presents the deposition fluxes across respiratory regions (head, TB, pulmonary) and the relative contributions of inhaled PFAS associated with coarse, fine, and ultrafine particles. The majority of PFAS measured exhibited similar size distributions, with most particles falling within the fine fraction (0.1 – 2.5 μm), resulting in broadly consistent deposition patterns. The average total deposition flux across these PFAS was $5.3 \pm 1.0 \text{ pg h}^{-1}$, with deposition distributed relatively evenly between the head ($23\% \pm 2\%$, 1.22 pg h^{-1}), TB ($26\% \pm 1\%$, 1.34 pg h^{-1}), and pulmonary ($40\% \pm 1\%$, 2.08 pg h^{-1}) regions.

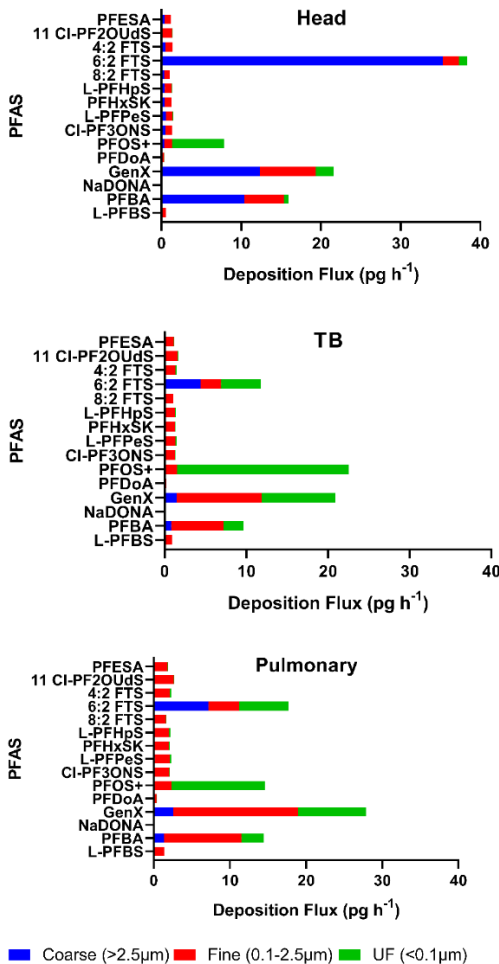


Figure 4: Modelled fractional deposition flux (pg h⁻¹) in the Pulmonary, Tracheobronchial (TB) and Head regions of the human respiratory tract.



407 PFDoA and NaDONA were notable exceptions due to their significantly lower aerosol concentrations, resulting in total
 408 deposition fluxes of 1.18 pg h^{-1} and 0.138 pg h^{-1} , respectively. PFDoA's size distribution was similar to the majority, yielding
 409 comparable regional deposition: 29% to the head (0.34 pg h^{-1}), 22% to the TB region (0.26 pg h^{-1}), and 36% to the pulmonary
 410 region (0.43 pg h^{-1}). NaDONA however exhibited an additional peak in the coarse fraction, shifting deposition toward the head
 411 region, which received 57% of the total flux (0.08 pg h^{-1}), while the TB and pulmonary regions received 13% (0.02 pg h^{-1}) and
 412 21% (0.03 pg h^{-1}), respectively. PFOS and PFBA showed significantly higher aerosol concentrations, with total deposition
 413 fluxes of 48.1 pg h^{-1} and 44.3 pg h^{-1} , respectively. PFBA had a similar size distribution to the majority but at higher
 414 concentration, resulting in deposition fractions of 36% to the head (15.9 pg h^{-1}), 22% to the TB region (9.7 pg h^{-1}), and 33%
 415 to the pulmonary region (14.5 pg h^{-1}). PFOS, however, had an additional peak in the ultrafine range, shifting deposition toward
 416 the TB region, which received 47% of the total flux (22.5 pg h^{-1}), while the head region received 16% (7.9 pg h^{-1}). GenX and
 417 6:2 FTS exhibited the highest aerosol concentrations and deposition fluxes, at 77.5 pg/h and 74.4 pg h^{-1} , respectively. GenX
 418 followed the typical deposition pattern, with 28% to the head (21.6 pg h^{-1}), 27% to the TB region (20.9 pg h^{-1}), and 36% to the
 419 pulmonary region (27.9 pg h^{-1}). In contrast, 6:2 FTS had additional modes in both the ultrafine and coarse fractions, leading to
 420 a deposition profile skewed toward the head region, which received 52% of the total flux (38.4 pg/h), while the TB and
 421 pulmonary regions received 16% (11.8 pg h^{-1}) and 24% (17.7 pg h^{-1}), respectively. This pattern was similar to that observed
 422 for NaDONA.

423 Particle deposition in the respiratory tract is primarily governed by inertial impaction, gravitational sedimentation, and
 424 Brownian diffusion, each dominating in different regions depending on particle size and airflow. Coarse particles deposit
 425 mainly in the upper airways via impaction and sedimentation, while ultrafine particles reach the distal pulmonary region
 426 through diffusion. Modelled deposition efficiencies by size and region are provided in the SI. Comparing the relative
 427 contribution to the deposition flux of the inhaled PFAS associated with the different size fractions, coarse particles showed the
 428 highest deposition flux in the head region ($60\% \pm 3\%$), with lower contributions to the pulmonary ($15\% \pm 2\%$) and
 429 tracheobronchial ($3\% \pm 8\%$) regions. Fine particles ($0.1\text{--}2.5 \mu\text{m}$), which dominate the PFAS size distribution, had the lowest
 430 overall deposition efficiency but were more evenly distributed: $39\% \pm 10\%$ to the pulmonary region, $25\% \pm 7\%$ to TB, and
 431 $18\% \pm 5\%$ to the head. Ultrafine particles shifted deposition toward the pulmonary region ($45\% \pm 14\%$), with $35\% \pm 11\%$ to
 432 TB and only $8\% \pm 3\%$ to the head.

433 The modelled deposition behaviour of PFAS compounds investigated is closely linked to their particle size distribution. PFOS,
 434 GenX, 6:2 FTS, and PFBA exhibited significant ultrafine fractions, suggesting a higher likelihood of deep lung penetration.
 435 This is particularly concerning given that clearance mechanisms in the pulmonary region are slower compared to upper
 436 airways, and pulmonary deposition increases the potential for translocation into the bloodstream. These findings highlight the
 437 importance of considering both particle size and regional deposition when assessing inhalation exposure risks, especially for
 438 compounds with known toxicological profiles and environmental persistence.



439 4 Conclusions

440 This study examined the aerosol formation and size-resolved distribution of a range of PFAS under controlled chamber
441 conditions, using mixed water–organic systems with and without the model bacterium *Pseudomonas fluorescens* to assess the
442 influence of molecular structure, interfacial behaviour and biological material on aerosol properties.
443 In terms of aerosolisation efficiency, sulfonated PFAS exhibited broadly similar aerosol-phase concentrations across chain
444 lengths, whereas perfluoroalkyl carboxylic acids showed increasing aerosolisation with increasing chain length, highlighting
445 the influence of functional group and hydrophobicity on the overall transfer of PFAS into the particle phase.
446 Most PFAS were associated with the fine aerosol mode, displaying unimodal mass–size distributions centred near 0.3 μm .
447 This consistent fine-mode behaviour across PFAS of differing chain lengths and functional groups indicates that aerosol
448 formation was governed primarily by physical processes of droplet generation and evaporation. PFOS showed enhanced
449 ultrafine enrichment, while 6:2 FTS and NaDONA displayed broader profiles, suggesting that differences in volatility and
450 interfacial behaviour introduce secondary compound-specific effects.
451 The presence of *Pseudomonas fluorescens* as an aerosol seed did not enhance PFAS aerosolisation or alter modal diameters,
452 but resulted in small, compound-specific reductions, particularly for PFEESA and GenX. The absence of PFAS enrichment at
453 the bacterial modal diameter ($\sim 0.6 \mu\text{m}$) indicates limited association of PFAS with bacterial surfaces under the tested
454 conditions, likely reflecting electrostatic repulsion and preferential stabilisation of PFAS at air–liquid interfaces. These results
455 suggest that biological material exerts only a minor influence on PFAS partitioning through the airborne pathway examined
456 here; however, aqueous-phase sorption or complexation before aerosolisation may still contribute to water-to-air transfer and
457 warrants further investigation. Moreover, if similar behaviour holds in the atmosphere, surface-active PFAS may avoid shifting
458 into bioaerosol particle sizes with higher deposition velocities and therefore remain in the fine aerosol range with longer
459 atmospheric lifetimes and transport potential.
460 MPPD simulations using the experimental size distributions indicated that most aerosol-bound PFAS would deposit in the
461 pulmonary region. Compounds with stronger ultrafine enrichment, including PFOS, 6:2 FTS and GenX, showed higher
462 predicted deposition in distal lung regions where clearance is slow and transfer into epithelial lining fluids is more likely.
463 Under the studied conditions, PFAS-containing aerosols therefore fall largely within respirable size ranges relevant to
464 inhalation exposure.
465 Overall, PFAS aerosolisation and particle-phase behaviour in the mixed solvent system were dominated by the physical
466 processes of droplet formation and evaporation, suggesting that engineering and operational measures that suppress fine droplet
467 production could reduce airborne PFAS emissions. The observed fine-mode distributions also imply that aerosolised PFAS
468 may be efficiently transported in the atmosphere and contribute to inhalation exposure beyond immediate emission sources.
469 Although the water–methanol system does not fully reflect environmental conditions, it provides a controlled basis for
470 identifying the fundamental processes governing PFAS transfer from contaminated aqueous systems to air.



471 Future work should apply this framework to more environmentally representative matrices, including natural organic matter,
472 and diverse microbial assemblages, to better capture real emission complexity. Combining controlled chamber experiments
473 with field measurements of size-resolved PFAS and bioaerosol emissions will be essential for improving predictions of PFAS
474 atmospheric transport, deposition and human exposure.

475 **5 Financial Support**

476 This work was supported by the European Commission, Horizon 2020 Research Infrastructures (EUROCHAMP-2020) Trans
477 National Access grant ATMO-TNA-6M-0000000034, “Investigation of the aerosolisation dynamics and biological
478 interactions of GenX “forever chemicals” – AEROBIOGEN”. The authors gratefully acknowledge the Coventry University
479 QR funding for supporting the Trailblazers PhD studentship awarded to JPK, secured by IK, and also thank CAWR at Coventry
480 University for its financial assistance.

481 **6 Competing Interests**

482 Some authors are members of the editorial board of journal ACP. The authors have no other competing interests to declare.

483 **7 Author Contributions**

484 IK, SC, FM, EG, DM, PP conceived the study. IK, JPK, SC, FM, DM, EG, VV performed lab measurements, sampling, and
485 sample analysis. IK, JPK, FM, EG performed data processing and interpretation. AB performed modelling. IK, JPK, FM, AB
486 prepared the original draft of the paper. All authors contributed to reviewing and editing the manuscript.

487 **8 Data Availability**

488 The dataset for this work can be accessed at DOI 10.5281/zenodo.17756209

489 **9 References**

- 490 Ahrens, L., Shoeib, M., Harner, T., Lee, S. C., Guo, R., and Reiner, E. J.: Wastewater Treatment Plant and Landfills as Sources
491 of Polyfluoroalkyl Compounds to the Atmosphere, *Environ. Sci. Technol.*, 45, 8098-8105, <https://doi.org/10.1021/es1036173>,
492 2011.
- 493 Alves, A. V., Tsianou, M., and Alexandridis, P.: Fluorinated Surfactant Adsorption on Mineral Surfaces: Implications for
494 PFAS Fate and Transport in the Environment, *Surfaces*, 3(4), 516-566, <https://doi.org/10.3390/surfaces3040037>, 2020.



- 495 Anjilvel, S. and Asgharian, B.: A Multiple-Path Model of Particle Deposition in the Rat Lung, *Fundam. Appl. Toxicol.*, 28,
 496 41-50, <https://doi.org/10.1006/faat.1995.1144>, 1995.
- 497 Barber, J. L., Berger, U., Chaemfa, C., Huber, S., Jahnke, A., Temme, C., and Jones, K. C.: Analysis of per- and polyfluorinated
 498 alkyl substances in air samples from Northwest Europe, *J. Environ. Monit.*, 9, 530-541, <https://doi.org/10.1039/B701417A>,
 499 2007.
- 500 Boyd Chelsea, D., Smith, T. J., El-Kirat-Chatel, S., Newell Peter, D., Dufrêne Yves, F., and O'Toole George, A.: Structural
 501 Features of the *Pseudomonas fluorescens* Biofilm Adhesin LapA Required for LapG-Dependent Cleavage, Biofilm Formation,
 502 and Cell Surface Localization, *J. Bacteriol.*, 196, 2775-2788, <https://doi.org/10.1128/jb.01629-14>, 2014.
- 503 Cai, W., Navarro, D. A., Du, J., Ying, G., Yang, B., McLaughlin, M. J., and Kookana, R. S.: Increasing ionic strength and
 504 valency of cations enhance sorption through hydrophobic interactions of PFAS with soil surfaces, *Sci. Total Environ.*, 817,
 505 152975, <https://doi.org/10.1016/j.scitotenv.2022.152975>, 2022.
- 506 Cheong, W. J. and Carr, P. W.: The Surface Tension of Mixtures of Methanol, Acetonitrile, Tetrahydrofuran, Isopropanol,
 507 Tertiary Butanol and Dimethyl-Sulfoxide with Water at °C, *J. Liq. Chromatogr.*, 10, 561-581,
 508 <https://doi.org/10.1080/01483918708069009>, 1987.
- 509 Charlton, S. G. V., Jana, S., and Chen, J.: Yielding behaviour of chemically treated *Pseudomonas fluorescens* biofilms,
 510 *Biofilm*, 8, 100209, <https://doi.org/10.1016/j.biofilm.2024.100209>, 2024.
- 511 Cookson, E. S. and Detwiler, R. L.: Global patterns and temporal trends of perfluoroalkyl substances in municipal wastewater:
 512 A meta-analysis, *Water Res.*, 221, 118784, <https://doi.org/10.1016/j.watres.2022.118784>, 2022.
- 513 Dai, M., Yan, N., and Brusseau, M. L.: Potential impact of bacteria on the transport of PFAS in porous media, *Water Res.*,
 514 243, 120350, <https://doi.org/10.1016/j.watres.2023.120350>, 2023.
- 515 Després, V., Huffman, J. A., Burrows, S. M., Hoose, C., Safatov, A., Buryak, G., Fröhlich-Nowoisky, J., Elbert, W., Andreae,
 516 M., Pöschl, U., and Jaenicke, R.: Primary biological aerosol particles in the atmosphere: a review, *Tellus B*, 64, 15598,
 517 <https://doi.org/10.3402/tellusb.v64i0.15598>, 2012.
- 518 Dreyer, A., Kirchgeorg, T., Weinberg, I., and Matthias, V.: Particle-size distribution of airborne poly- and perfluorinated alkyl
 519 substances, *Chemosphere*, 129, 142-149, <https://doi.org/10.1016/j.chemosphere.2014.06.069>, 2015.
- 520 Engvall, A. C., Krejci, R., Ström, J., Treffeisen, R., Scheele, R., Hermansen, O., and Paatero, J.: Changes in aerosol properties
 521 during spring-summer period in the Arctic troposphere, *Atmos. Chem. Phys.*, 8, 445-462, <https://doi.org/10.5194/acp-8-445->
 522 2008, 2008.



- 523 Ellis, D. A., Martin, J. W., De Silva, A. O., Mabury, S. A., Hurley, M. D., Sulbaek Andersen, M. P., and Wallington, T. J.:
 524 Degradation of Fluorotelomer Alcohols: A Likely Atmospheric Source of Perfluorinated Carboxylic Acids, *Environ. Sci.*
 525 *Technol.*, 38, 3316-3321, <https://doi.org/10.1021/es049860w>, 2004.
- 526 Ervens, B. and Amato, P.: The global impact of bacterial processes on carbon mass, *Atmos. Chem. Phys.*, 20, 1777-1794,
 527 <https://doi.org/10.5194/acp-20-1777-2020>, 2020.
- 528 Estillore, A. D., Trueblood, J. V., and Grassian, V. H.: Atmospheric chemistry of bioaerosols: heterogeneous and multiphase
 529 reactions with atmospheric oxidants and other trace gases, *Chem. Sci.*, 7, 6604-6616, <https://doi.org/10.1039/C6SC02353C>,
 530 2016.
- 531 Evich, M. G., Davis, M. J. B., McCord, J. P., Acrey, B., Awkerman, J. A., Knappe, D. R. U., Lindstrom, A. B., Speth, T. F.,
 532 Tebes-Stevens, C., Strynar, M. J., Wang, Z., Weber, E. J., Henderson, W. M., and Washington, J. W.: Per- and polyfluoroalkyl
 533 substances in the environment, *Science*, 375, eabg9065, <https://doi.org/10.1126/science.abg9065>, 2022.
- 534 Farmer, D. K., Boedicker, E. K., and DeBolt, H. M.: Dry Deposition of Atmospheric Aerosols: Approaches, Observations,
 535 and Mechanisms, *Annu. Rev. Phys. Chem.*, 72, 375-397, <https://doi.org/10.1146/annurev-physchem-090519-034936>, 2021.
- 536 Fathollahi, A. and Coupe, S. J.: Effect of environmental and nutritional conditions on the formation of single and mixed-
 537 species biofilms and their efficiency in cadmium removal, *Chemosphere*, 283, 131152,
 538 <https://doi.org/10.1016/j.chemosphere.2021.131152>, 2021.
- 539 Faust, J. A.: PFAS on atmospheric aerosol particles: a review, *Environ. Sci.: Processes Impacts*, 25, 133-150,
 540 <https://doi.org/10.1039/D2EM00002D>, 2023.
- 541 Finlayson-Pitts, B. J. and Pitts, J.N.: *Chemistry of the Upper and Lower Atmosphere: Theory, Experiments, and Applications*,
 542 Academic Press, 298–299, San Diego, CA, 2000.
- 543 Folorunsho, O., Bogush, A., and Kourtchev, I.: Investigation of Per- and Polyfluoroalkyl Substances (PFAS) Adsorption onto
 544 the Medium Size Quartz Gravel, *Environ. Contam. Causes Solutions.*, 1, 4, <https://doi.org/10.53941/eccs.2025.100004>, 2025.
- 545 Fröhlich-Nowoisky, J., Kampf, C. J., Weber, B., Huffman, J. A., Pöhlker, C., Andreae, M. O., Lang-Yona, N., Burrows, S.
 546 M., Gunthe, S. S., Elbert, W., Su, H., Hoor, P., Thines, E., Hoffmann, T., Després, V. R., and Pöschl, U.: Bioaerosols in the
 547 Earth system: Climate, health, and ecosystem interactions, *Atmos. Res.*, 182, 346-376,
 548 <https://doi.org/10.1016/j.atmosres.2016.07.018>, 2016.
- 549 Gatta, E., Abd El, E., Brunoldi, M., Irfan, M., Isolabella, T., Massabò, D., Parodi, F., Prati, P., Vernocchi, V., and Mazzei, F.:
 550 Viability studies of bacterial strains exposed to nitrogen oxides and light in controlled atmospheric conditions, *Sci. Rep.*, 15,
 551 10320, <https://doi.org/10.1038/s41598-025-94898-y>, 2025.



- 552 Ge, H., Yamazaki, E., Yamashita, N., Taniyasu, S., Ogata, A., and Furuuchi, M.: Particle size specific distribution of perfluoro
 553 alkyl substances in atmospheric particulate matter in Asian cities, *Environ. Sci.: Processes Impacts.*, 19, 549-560,
 554 <https://doi.org/10.1039/C6EM00564K>, 2017.
- 555 Glüge, J., Scheringer, M., Cousins, I. T., DeWitt, J. C., Goldenman, G., Herzke, D., Lohmann, R., Ng, C. A., Trier, X., and
 556 Wang, Z.: An overview of the uses of per- and polyfluoroalkyl substances (PFAS), *Environ. Sci.: Processes Impacts.*, 22,
 557 2345-2373, <https://doi.org/10.1039/D0EM00291G>, 2020.
- 558 Guo, M., Lyu, Y., Xu, T., Yao, B., Song, W., Li, M., Yang, X., Cheng, T., and Li, X.: Particle size distribution and respiratory
 559 deposition estimates of airborne perfluoroalkyl acids during the haze period in the megacity of Shanghai, *Environ. Pollut.*,
 560 234, 9-19, <https://doi.org/10.1016/j.envpol.2017.10.128>, 2018.
- 561 Guo, B., Saleem, H., and Brusseau, M. L.: Predicting Interfacial Tension and Adsorption at Fluid–Fluid Interfaces for Mixtures
 562 of PFAS and/or Hydrocarbon Surfactants, *Environ. Sci. Technol.*, 57, 8044-8052, <https://doi.org/10.1021/acs.est.2c08601>,
 563 2023.
- 564 Harada, K., Nakanishi, S., Sasaki, K., Furuyama, K., Nakayama, S., Saito, N., Yamakawa, K., and Koizumi, A.: Particle Size
 565 Distribution and Respiratory Deposition Estimates of Airborne Perfluorooctanoate and Perfluorooctanesulfonate in Kyoto
 566 Area, Japan, *Bull. Environ. Contam. Toxicol.*, 76, 306-310, <https://doi.org/10.1007/s00128-006-0922-1>, 2006.
- 567 Hong, S., Kim, M.-W., and Jang, J.: Physical collection and viability of airborne bacteria collected under electrostatic field
 568 with different sampling media and protocols towards rapid detection, *Sci. Rep.*, 11, 14598, [https://doi.org/10.1038/s41598-](https://doi.org/10.1038/s41598-021-94033-7)
 569 021-94033-7, 2021.
- 570 Johansson, J. H., Salter, M. E., Acosta Navarro, J. C., Leck, C., Nilsson, E. D., and Cousins, I. T.: Global transport of
 571 perfluoroalkyl acids via sea spray aerosol, *Environ. Sci.: Processes Impacts.*, 21, 635-649,
 572 <https://doi.org/10.1039/C8EM00525G>, 2019.
- 573 Key, B. D., Howell, R. D., and Criddle, C. S.: Defluorination of Organofluorine Sulfur Compounds by *Pseudomonas* Sp. Strain
 574 D2, *Environ. Sci. Technol.*, 32, 2283-2287, <https://doi.org/10.1021/es9800129>, 1998.
- 575 Klevan, C., Van Allen, O., Xia, S., Mukai, K., Gomes, A., Caines, S., Woodcock, M. J., and Pennell, K. D.: Evaluation of co-
 576 foaming agents for enhanced removal of per- and polyfluoroalkyl substances (PFAS) by foam fractionation, *J. Hazard. Mater.*,
 577 494, 138423, <https://doi.org/10.1016/j.jhazmat.2025.138423>, 2025.
- 578 Kourtchev, I., McGillen, M. R., Wenger, J., and Donahue, N. M.: Rethinking environmental boundaries for contaminants of
 579 emerging concern, *Atmos. Environ.*, 361, 121492, <https://doi.org/10.1016/j.atmosenv.2025.121492>, 2025.
- 580 Kourtchev, I., Hellebust, S., Heffernan, E., Wenger, J., Towers, S., Diapouli, E., and Eleftheriadis, K.: A new on-line SPE LC-
 581 HRMS method for the analysis of Perfluoroalkyl and Polyfluoroalkyl Substances (PFAS) in PM_{2.5} and its application for



- 582 screening atmospheric particulates from Dublin and Enniscorthy, Ireland, *Sci. Total Environ.*, 835, 155496,
583 <https://doi.org/10.1016/j.scitotenv.2022.155496>, 2022.
- 584 Kourtchev, I., Sebben, B. G., Brill, S., Barbosa, C. G. G., Weber, B., Ferreira, R. R., D'Oliveira, F. A. F., Dias-Junior, C. Q.,
585 Popoola, O. A. M., Williams, J., Pöhlker, C., and Godoi, R. H. M.: Occurrence of a “forever chemical” in the atmosphere
586 above pristine Amazon Forest, *Sci. Total Environ.*, 944, 173918, <https://doi.org/10.1016/j.scitotenv.2024.173918>, 2024.
- 587 Kutsuna, S., Hori, H., Sonoda, T., Iwakami, T., and Wakisaka, A.: Preferential solvation of perfluorooctanoic acid (PFOA) by
588 methanol in methanol–water mixtures: A potential overestimation of the dissociation constant of PFOA using a Yasuda–
589 Shedlovsky plot, *Atmos. Environ.*, 49, 411–414, <https://doi.org/10.1016/j.atmosenv.2011.12.009>, 2012.
- 590 Leung, S. C. E., Wanninayake, D., Chen, D., Nguyen, N.-T., and Li, Q.: Physicochemical properties and interactions of
591 perfluoroalkyl substances (PFAS) - Challenges and opportunities in sensing and remediation, *Sci. Total Environ.*, 905, 166764,
592 <https://doi.org/10.1016/j.scitotenv.2023.166764>, 2023.
- 593 Li, J., Zhou, L., Zhang, X., Xu, C., Dong, L., and Yao, M.: Bioaerosol emissions and detection of airborne antibiotic resistance
594 genes from a wastewater treatment plant, *Atmos. Environ.*, 124, 404–412, <https://doi.org/10.1016/j.atmosenv.2015.06.030>,
595 2016.
- 596 Lin, H., Lao, J.-Y., Wang, Q., Ruan, Y., He, Y., Lee, P. K. H., Leung, K. M. Y., and Lam, P. K. S.: Per- and polyfluoroalkyl
597 substances in the atmosphere of waste management infrastructures: Uncovering secondary fluorotelomer alcohols, particle
598 size distribution, and human inhalation exposure, *Environ. Int.*, 167, 107434, <https://doi.org/10.1016/j.envint.2022.107434>,
599 2022.
- 600 Luczkiewicz, A., Kotlarska, E., Artichowicz, W., Tarasewicz, K., and Fudala-Ksiazek, S.: Antimicrobial resistance of
601 *Pseudomonas* spp. isolated from wastewater and wastewater-impacted marine coastal zone, *Environ. Sci. Pollut. Res.*, 22,
602 19823–19834, <https://doi.org/10.1007/s11356-015-5098-y>, 2015.
- 603 Lyu, Y., Wang, B., Du, X., Guo, B., and Brusseau, M. L.: Air–water interfacial adsorption of C4–C10 perfluorocarboxylic
604 acids during transport in unsaturated porous media, *Sci. Total Environ.*, 831, 154905,
605 <https://doi.org/10.1016/j.scitotenv.2022.154905>, 2022.
- 606 Massabò, D., Danelli, S. G., Brotto, P., Comite, A., Costa, C., Di Cesare, A., Doussin, J. F., Ferraro, F., Formenti, P., Gatta,
607 E., Negretti, L., Oliva, M., Parodi, F., Vezzulli, L., and Prati, P.: ChAMBRé: a new atmospheric simulation chamber for aerosol
608 modelling and bio-aerosol research, *Atmos. Meas. Tech.*, 11, 5885–5900, <https://doi.org/10.5194/amt-11-5885-2018>, 2018.
- 609 Pandamkulangara Kizhakkethil, J. and Kourtchev, I.: Aerosolisation of new generation perfluoroalkyl ether carboxylic and
610 sulfonic acids from aeration of contaminated aqueous solutions, *Atmos. Environ.*, 352, 121218,
611 <https://doi.org/10.1016/j.atmosenv.2025.121218>, 2025.



- 612 Pandamkulangara Kizhakkethil, J., Shi, Z., Bogush, A., and Kourtchev, I.: Aerosolisation of per- and polyfluoroalkyl
 613 substances (PFAS) during aeration of contaminated aqueous solutions, *Atmos. Environ.*, 334, 120716,
 614 <https://doi.org/10.1016/j.atmosenv.2024.120716>, 2024.
- 615 Pandamkulangara Kizhakkethil, J., Shi, Z., Bogush, A., and Kourtchev, I.: Measurement report: Per- and polyfluoroalkyl
 616 substances (PFAS) in particulate matter (PM10) from activated sludge aeration, *Atmos. Chem. Phys.*, 25, 5947-5958,
 617 <https://doi.org/10.5194/acp-25-5947-2025>, 2025.
- 618 Park, D., Kim, Y. H., Woo Park, C., Hwang, J., and Kim, Y. J.: New bio-aerosol collector using a micromachined virtual
 619 impactor, *J Aerosol Sci*, 40, 415–422, <https://doi.org/10.1016/J.JAEROSCI.2008.12.007>, 2009.
- 620 Patel, R., Saab, L. E., Brahana, P. J., Valsaraj, K. T., and Bharti, B.: Interfacial Activity and Surface pKa of Perfluoroalkyl
 621 Carboxylic Acids (PFCAs), *Langmuir*, 40, 3651-3658, <https://doi.org/10.1021/acs.langmuir.3c03398>, 2024.
- 622 Poopedi, E., Pierneef, R., Singh, T., and Gomba, A.: Opportunistic bacterial pathogens in bioaerosols emitted at municipal
 623 wastewater treatment plants, South Africa, *Sci. Rep.*, 15, 10318, <https://doi.org/10.1038/s41598-025-95484-y>, 2025.
- 624 Pope III, C. A. and Dockery, D. W.: Health Effects of Fine Particulate Air Pollution: Lines that Connect, *Air Waste Manage.*
 625 *Assoc. J.*, 56, 709-742, <https://doi.org/10.1080/10473289.2006.10464485>, 2006.
- 626 Reth, M., Berger, U., Broman, D., Cousins, I. T., Nilsson, E. D., and McLachlan, M. S.: Water-to-air transfer of perfluorinated
 627 carboxylates and sulfonates in a sea spray simulator, *Environ. Chem.*, 8, 381-388, <https://doi.org/10.1071/EN11007>, 2011.
- 628 Romakkaniemi, S., Kokkola, H., Smith, J. N., Prisle, N. L., Schwier, A. N., McNeill, V. F., and Laaksonen, A.: Partitioning
 629 of semivolatile surface-active compounds between bulk, surface and gas phase, *Geophys. Res. Lett.*, 38,
 630 <https://doi.org/10.1029/2010GL046147>, 2011.
- 631 Schaefer, C. E., Culina, V., Nguyen, D., and Field, J.: Uptake of Poly- and Perfluoroalkyl Substances at the Air–Water
 632 Interface, *Environ. Sci. Technol.*, 53, 12442-12448, <https://doi.org/10.1021/acs.est.9b04008>, 2019.
- 633 Schenker, U., Scheringer, M., MacLeod, M., Martin, J. W., Cousins, I. T., and Hungerbühler, K.: Contribution of Volatile
 634 Precursor Substances to the Flux of Perfluorooctanoate to the Arctic, *Environ. Sci. Technol.*, 42, 3710-3716,
 635 <https://doi.org/10.1021/es703165m>, 2008.
- 636 Sha, B., Johansson, J. H., Benskin, J. P., Cousins, I. T., and Salter, M. E.: Influence of Water Concentrations of Perfluoroalkyl
 637 Acids (PFAAs) on Their Size-Resolved Enrichment in Nascent Sea Spray Aerosols, *Environ. Sci. Technol.*, 55, 9489-9497,
 638 <https://doi.org/10.1021/acs.est.0c03804>, 2021.
- 639 Sha, B., Ungerovich, E., Salter, M. E., Cousins, I. T., and Johansson, J. H.: Enrichment of Perfluoroalkyl Acids on Sea Spray
 640 Aerosol in Laboratory Experiments: The Role of Dissolved Organic Matter, Air Entrainment Rate and Inorganic Ion
 641 Composition, *Environ. Sci. Technol. Lett.*, 11, 746-751, <https://doi.org/10.1021/acs.estlett.4c00287>, 2024.



- 642 Shoeib, M., Schuster, J., Rauert, C., Su, K., Smyth, S.-A., and Harner, T.: Emission of poly and perfluoroalkyl substances,
 643 UV-filters and siloxanes to air from wastewater treatment plants, *Environ. Pollut.*, 218, 595-604,
 644 <https://doi.org/10.1016/j.envpol.2016.07.043>, 2016.
- 645 Sillankorva, S., Neubauer, P., and Azeredo, J.: Isolation and characterization of a T7-like lytic phage for *Pseudomonas*
 646 *fluorescens*, *BMC Biotechnol.*, 8, 80, <https://doi.org/10.1186/1472-6750-8-80>, 2008.
- 647 Steele, W. V., Chirico, R. D., Knipmeyer, S. E., and Nguyen, A.: Vapor Pressure, Heat Capacity, and Density along the
 648 Saturation Line: Measurements for Benzenamine, Butylbenzene, sec-Butylbenzene, tert-Butylbenzene, 2,2-Dimethylbutanoic
 649 Acid, Tridecafluoroheptanoic Acid, 2-Butyl-2-ethyl-1,3-propanediol, 2,2,4-Trimethyl-1,3-pentanediol, and 1-Chloro-2-
 650 propanol, *J. Chem. Eng. Data.*, 47, 648-666, <https://doi.org/10.1021/je010083e>, 2002.
- 651 Stolzenburg, D., Fischer, L., Vogel, A. L., Heinritzi, M., Schervish, M., Simon, M., Wagner, A. C., Dada, L., Ahonen, L. R.,
 652 Amorim, A., Baccarini, A., Bauer, P. S., Baumgartner, B., Bergen, A., Bianchi, F., Breitenlechner, M., Brilke, S., Buenrostro
 653 Mazon, S., Chen, D., Dias, A., Draper, D. C., Duplissy, J., El Haddad, I., Finkenzeller, H., Frege, C., Fuchs, C., Garmash, O.,
 654 Gordon, H., He, X., Helm, J., Hofbauer, V., Hoyle, C. R., Kim, C., Kirkby, J., Kontkanen, J., Kürten, A., Lampilahti, J.,
 655 Lawler, M., Lehtipalo, K., Leiminger, M., Mai, H., Mathot, S., Mentler, B., Molteni, U., Nie, W., Nieminen, T., Nowak, J. B.,
 656 Ojdanic, A., Onnela, A., Passananti, M., Petäjä, T., Quéléver, L. L. J., Rissanen, M. P., Sarnela, N., Schallhart, S., Tauber, C.,
 657 Tomé, A., Wagner, R., Wang, M., Weitz, L., Wimmer, D., Xiao, M., Yan, C., Ye, P., Zha, Q., Baltensperger, U., Curtius, J.,
 658 Dommen, J., Flagan, R. C., Kulmala, M., Smith, J. N., Worsnop, D. R., Hansel, A., Donahue, N. M., and Winkler, P. M.:
 659 Rapid growth of organic aerosol nanoparticles over a wide tropospheric temperature range, *Proc. Natl. Acad. Sci. U.S.A.*, 115,
 660 9122-9127, <https://doi.org/10.1073/pnas.1807604115>, 2018.
- 661 Torres, E.: Biosorption: A Review of the Latest Advances, *Processes*, 8, 1584 <https://doi.org/10.3390/pr8121584>, 2020.
- 662 Tsuda, A., Henry, F. S., and Butler, J. P.: Particle Transport and Deposition: Basic Physics of Particle Kinetics, *Compr.*
 663 *Physiol.*, 3, 1437-1471, <https://doi.org/10.1002/j.2040-4603.2013.tb00526.x>, 2013.
- 664 Ungeheuer, F., Caudillo, L., Ditas, F., Simon, M., van Pinxteren, D., Kılıç, D., Rose, D., Jacobi, S., Kürten, A., Curtius, J., and
 665 Vogel, A. L.: Nucleation of jet engine oil vapours is a large source of aviation-related ultrafine particles, *Commun. Earth*
 666 *Environ.*, 3, 319, <https://doi.org/10.1038/s43247-022-00653-w>, 2022.
- 667 US EPA: Estimation Programs Interface Suite™ for Microsoft® Windows, v 4.11: [https://www.epa.gov/tsca-screening-](https://www.epa.gov/tsca-screening-tools/epi-suitetm-estimation-program-interface)
 668 [tools/epi-suitetm-estimation-program-interface](https://www.epa.gov/tsca-screening-tools/epi-suitetm-estimation-program-interface), 2012. last access: 08th November 2025.
- 669 US EPA: Drinking Water Health Advisory: Hexafluoropropylene Oxide (HFPO) Dimer Acid (CASRN 13252-13-6) and HFPO
 670 Dimer Acid Ammonium Salt (CASRN 62037-80-3), Also Known as “GenX Chemicals”:
 671 <https://www.epa.gov/system/files/documents/2022-06/drinking-water-genx-2022.pdf>, 2022. last access: 08th November 2025.



- 672 Vernocchi, V., Abd El, E., Brunoldi, M., Danelli, S. G., Gatta, E., Isolabella, T., Mazzei, F., Parodi, F., Prati, P., and Massabò,
673 D.: Airborne bacteria viability and air quality: a protocol to quantitatively investigate the possible correlation by an atmospheric
674 simulation chamber, *Atmos. Meas. Tech.*, 16, 5479-5493, <https://doi.org/10.5194/amt-16-5479-2023>, 2023.
- 675 Wang, J. and Chen, C.: Biosorbents for heavy metals removal and their future, *Biotechnol. Adv.*, 27, 195-226,
676 <https://doi.org/10.1016/j.biotechadv.2008.11.002>, 2009.
- 677 Wanzek, T., Stults, J. F., Johnson, M. G., Field, J. A., and Kleber, M.: Role of Mineral–Organic Interactions in PFAS Retention
678 by AFFF-Impacted Soil, *Environ. Sci. Technol.*, 57, 5231-5242, <https://doi.org/10.1021/acs.est.2c08806>, 2023.
- 679 Wu, W., Jin, Y., and Carlsten, C.: Inflammatory health effects of indoor and outdoor particulate matter, *J. Allergy Clin.*
680 *Immunol.*, 141, 833-844, <https://doi.org/10.1016/j.jaci.2017.12.981>, 2018.
- 681 Xu, P., Zhang, C., Mou, X., and Wang, X. C.: Bioaerosol in a typical municipal wastewater treatment plant: concentration,
682 size distribution, and health risk assessment, *Water Science and Technology*, 82, 1547-1559,
683 <https://doi.org/10.2166/wst.2020.416>, 2020. *Water Sci. Technol.*
- 684 Zhang, L. and Vet, R.: A review of current knowledge concerning size-dependent aerosol removal, *China Particuology*, 4,
685 272-282, [https://doi.org/10.1016/S1672-2515\(07\)60276-0](https://doi.org/10.1016/S1672-2515(07)60276-0), 2006.